Materials Today Bio 15 (2022) 100326

Contents lists available at ScienceDirect

Materials Today Bio

journal homepage: www.journals.elsevier.com/materials-today-bio

Controllable graphene oxide-based biocompatible hybrid interface as an anti-fibrotic coating for metallic implants

Chong-You Chen [a,b,1], Pei-Hsuan Tsai [a,1], Ya-Hui Lin [a], Chien-Yu Huang [a,b], Johnson H.Y. Chung [c], Guan-Yu Chen [a,b,*]

[a] Institute of Biomedical Engineering, College of Electrical and Computer Engineering, National Yang Ming Chiao Tung University, Hsinchu, 300093, Taiwan
[b] Department of Electronics and Electrical Engineering, College of Electrical and Computer Engineering, National Yang Ming Chiao Tung University, Hsinchu, 300093, Taiwan
[c] ARC Centre of Excellence for Electromaterials Science, Intelligent Polymer Research Institute, University of Wollongong, Wollongong, NSW, 2500, Australia

ARTICLE INFO

Keywords:
Biocompatible hybrid interface
Graphene oxide
Implant materials
Anti-fibrotic effect
Surface roughness
Topological nanostructure

ABSTRACT

In tissue engineering, foreign body reactions (FBRs) that may occur after the insertion of medical implants are a considerable challenge. Materials currently used in implants are mainly metals that are non-organic, and the lack of biocompatibility and absence of immune regulations may lead to fibrosis after long periods of implantation. Here, we introduce a highly biocompatible hybrid interface of graphene oxide (GO) and collagen type I (COL-I), where the topological nanostructure can effectively inhibit the differentiation of fibroblasts into myofibroblasts. The structure and roughness of this coating interface can be easily adjusted at the nanoscale level through changes in the GO concentration, thereby effectively inducing the polarization of macrophages to the M1 state without producing excessive amounts of pro-inflammatory factors. Compared to nanomaterials or the extracellular matrix as an anti-fibrotic interface, this hybrid bio-interface has superior mechanical strength, physical structures, and high inflammation. Evidenced by inorganic materials such as glass, titanium, and nitinol, GO-COL shows great potential for use in medical implants and cell-material interfaces.

1. Introduction

The global demand for medically implantables is on the rise, with an increasing number of medical implants being inserted into human bodies each year with a compound annual growth rate of 13.69% [1]. However, most medical implants trigger unwanted foreign body reactions (FBRs) after implementation, which ultimately lead to fibrosis and irreversible damage to the device [2,3]. Once a biomaterial comes into contact with body fluids, proteins such as albumin, fibronectin, fibrinogen, and complements are immediately absorbed on the surface of implants. Protein deposition subsequently triggers the innate immune system, resulting in acute inflammation. Macrophages are one of the white cells first recruited to the implantation site, where they differentiate into the pro-inflammatory M1 phenotype and the alternative M2 phenotype [4]. Continuous stimulation of the implant site leads to chronic inflammation after a few days of acute inflammation. During chronic inflammation, the macrophages switch toward an alternatively activated M2 phenotype, and release pro-fibrotic factors such as the platelet-derived growth factor (PDGF) and transforming growth factor-β1 (TGF-β1) that stimulate conversion of fibroblasts into myofibroblasts [5,6]. These myofibroblasts produce extensive extracellular matrixes (ECMs), predominantly type I collagen (COL-I), resulting in a condensed fibrous capsule surrounding the implant. Macrophages play a crucial role in tissue regeneration by regulating the ECM environment, with excessive polarization of both M1/M2 phenotypes ending in fibrosis [7–10]. Therefore, regulating FBR from macrophage polarization in the tissue microenvironment is significant for the inhibition of fibrosis.

Surface modification is a common approach adopted to improve tissue integration by limiting severe FBR and fibrosis [11]. Biomaterials that resemble structures similar to natural ECM are better candidates for substrate coatings. Arg-Gly-Asp (RGD) motif-inhibiting coatings that could reduce cell adhesion, and slow-release drug coatings have been developed to inhibit implant fibrosis [12]. Other modifications target physical properties such as surface hydrophilicity, porosity, stiffness

*Corresponding author. Institute of Biomedical Engineering, College of Electrical and Computer Engineering, National Yang Ming Chiao Tung University, Hsinchu, 300093, Taiwan.
E-mail address: guanyu@nycu.edu.tw (G.-Y. Chen).
[1] The authors contributed equally to this work.

https://doi.org/10.1016/j.mtbio.2022.100326
Received 9 April 2022; Received in revised form 10 June 2022; Accepted 10 June 2022
Available online 15 June 2022

(elastic modulus), roughness and topography [13]. Recently, novel nano- and micro-patterning technologies have expanded the fundamental understanding of cellular behavior control [14–19]. Surfaces with nano-patterns have demonstrated great potential against fibrosis; the unique topology and roughness of the implant surfaces are sensed by fibroblasts that come in contact with them, resulting in inhibition of cell skeleton rearrangement and subsequent differentiation [15]. Although these approaches result in obvious inhibition of myofibroblasts, a lack of suitable immune regulation strategies still leads to fibrosis after prolonged implantation, with accumulated M2 macrophages continuing to attract and stimulate fibroblasts [6].

Graphene oxide (GO), a derivative of graphene, is composed of sp2 hybridized hexagonal lattice units, and exhibits a two-dimensional sheet-like structure [20]. Based on the abundant oxygen-containing functional groups (hydroxyl, epoxy, carbonyl, and carboxyl) on the surface, GO has been intensively investigated in the biomedical field such as in drug delivery, tissue engineering, wound healing and medical devices [21]. GO contains carbon radicals and possesses oxidative ability, and has been reported to induce a pro-inflammatory response through lipid peroxidation of the surface membrane as well as membrane damage and subcellular processing, especially in macrophages [22,23]. GO has also been evidenced to have an immunomodulatory influence on the pro-inflammatory, M1 phenotype of macrophages [24–26].

However, GO still faces significant challenges when applied to human bodies. Previous studies have reported dose-dependent cell death in several human cell lines including lung epithelial cells (BEAS-2B, A549), normal lung fibroblasts (HLF), and macrophages (THP-1) [22]. Although providing the GO with a coating makes it less toxic, there is still the risk of dissolution, release of GO flakes, and their cellular uptake. Therefore, researchers have incorporated GO in hydrogels to reduce its acute toxicity potential through the entrapment of GO in hydrogel matrices [27]. More importantly, GO can function as a coordinator to regulate the mechanical properties of hydrogels; the addition of GO significantly improves the tensile strength and modulus of elasticity of the hydrogel-based nanocomposite [27,28]. The covalent bond and interactions between GO and the polymers provide firm physical support [29,30].

In this study, we incorporated GO with COL-I to generate a biocompatible hybrid interface—the graphene oxide conjugated collagen (GO-COL) composite—demonstrating a coating surface with nanoscale roughness. By adjusting the GO concentration, the level of crosslinking in the GO-COL network as well as the surface roughness can be regulated. In addition, the oxidative ability of the GO flakes on this hybrid interface provides it a unique ability to inhibit fibrosis through immune regulation, and subsequently bestows anti-fibrotic properties on materials commonly used in implants such as glass, titanium, and nitinol.

2. Material and methods

2.1. Synthesis of GO-COL composites for use as coating

A single-layer GO solution was purchased from Sigma-Aldrich (#777676). According to the product information, GO was dissolved in water to obtain a concentration of 4 mg/mL. The average diameter of the GO flakes was approximately 400 nm.

To synthesize the GO and collagen complex, the 4 mg/mL GO stock solution was first diluted to 300 μg/mL in deionized water. Next, the gel linker N-(3-Dimethylaminopropyl)-N-ethyl carbodiimide hydrochloride (EDC, E1769, Sigma) and N-hydroxysulfosuccinimide sodium salt (NHS, FL-56485, Sigma) were added to the diluted GO solution and placed in a low-temperature ultrasonic cleaning machine and sonicated for 1 h to avoid uneven aggregation. Finally, COL-I purchased from Thermo Fisher (A1048301, Gibco) was added, and GO/(GO + COL) solutions of different weight percentages—in the sequence 8%,16%, and 32% GO-COL—were prepared.

2.2. X-ray photoelectron spectroscopy analysis

The X-ray photoelectron spectroscopy (XPS) spectra of GO, COL, 8% GO-COL, 16% GO-COL, and 32% GO-COL were obtained using the ESCALAB Xi+ (Thermo Fisher Scientific), and peak analyses were conducted using OriginPro 9.1 (OriginLab Corporation). All sample solutions were coated and dried on silicon wafers with at least five iterations.

2.3. Fourier transform infrared spectroscopy analysis

The measurements of functional changes among the 8%, 16%, and 32% GO-COL groups and COL were performed using Fourier transform infrared (FTIR) spectroscopy (Vertex 80v, Bruker). Solutions of 8%, 16%, and 32% GO-COL and COL were first prepared, after which all samples were coated and dried on silicon wafers, with at least five iterations performed.

2.4. Characterization of surface nanostructure and roughness

Scanning electron microscopy (SEM, SU-8010, Hitachi) was used to detect the surface nanostructures of the 8%, 16%, and 32% GO-COL samples as well as those of COL. Atomic force microscopy (AFM edge) was performed in tapping mode to record the surface roughness. For sample preparation, silicon wafers were placed overnight in the coating solution at 4 °C. The coated wafers were then washed with deionized water followed by fixation with 2.5% glutaraldehyde (G6257, Sigma) for 1 h. Subsequently, the samples were dehydrated with ethanol solution at 35%, 70%, 85%, and 99% concentrations, in that order (10 min at each concentration). After the removal of ethanol, the samples were soaked in 100% hexamethyldisilazane for 5 min and dried overnight at room temperature (RT).

2.5. Cell culture

The normal human lung fibroblast cell line (HFL-1) and the human monocytic cell line (THP-1) were acquired from the Bioresource Collection and Research Center (BCRC). The HFL-1 cell line was cultured in the Roswell Park Memorial Institute-1640 (RPMI-1640, Gibco) medium supplemented with 10% fetal bovine serum and 1% penicillin-streptomycin (P/S) in place of the F12K medium after the adaptation test. The THP-1 cell line was maintained in RPMI-1640 (Gibco) supplemented with 10% fetal bovine serum and 1% penicillin-streptomycin. All cell cultures were maintained in T75 flasks at 37 °C in an incubator with 5% CO_2.

For single culture, the glass slides, and Titanium disks (pure Ti, Ultimate Materials Technology Co., Ltd., Taiwan), or Nitinol disks (Ni 55% &Ti 45%, Ultimate Materials Technology Co., Ltd., Taiwan) were pre-coated with 8%, 16%, and 32% GO-COL, and COL by placing them overnight in the coating solution at 4 °C. HFL-1 cells were seeded on these glass slides, Titanium disks, or Nitinol disks and incubated for 24 h. THP-1 cells were also seeded on the coated glass slides, Titanium disks, or Nitinol disks; however, they were first cultured in RPMI-1640 medium with 150 nM PMA to induce differentiation. After 6 h of incubation, the suspension type THP-1 monocytes differentiated into an adhesive macrophage-like phenotype. The medium was then replaced with RPMI-1640 without PMA, and the cells incubated for 24 h.

For co-culture, the glass slides, Titanium disks, or Nitinol disks were also first pre-coated with 8%, 16%, and 32% GO-COL and COL by placing them overnight in the coating solution at 4 °C. Next, THP-1 cells were seeded using PMA treatment for 6 h. After that, the medium was replaced, and the HFL-1 fibroblasts were seeded together with macrophages in the ratio of 1:2 (macrophage: fibroblast = 1:2). Subsequently, the cells were cultured for 1, 3, or 7 days, depending on the experiment performed.

2.6. Cell viability

The reagent from the cell counting kit 8 (E-CK-A361, Elabscience) was applied to each well and incubated at 37 °C for 2 h. Single cell viability was measured at 24 h after approximately 2×10^4 THP-1 macrophages or 4×10^4 HFL-1 fibroblasts seeded onto GO-COL-coated coverslips in 24-well plates. The medium that underwent change of color was placed in the wells of a 96-well plate, with 100 μl per well and the absorbance was read using an ELISA reader. For co-culture, 2×10^4 THP-1 macrophages were initially seeded on GO-COL-coated coverslips in 24-well plates, and 4×10^4 HFL-1 fibroblasts were seeded after 6 h of macrophage adhesion. The viability of the co-culture was measured 24 h after both cells were seeded.

2.7. Immunofluorescence staining

The GO-COL coated 12 mm coverslips, Titanium disks, or Nitinol disks were placed at the bottom of 24-well plates. There were 2×10^4 THP-1 macrophages, 4×10^4 HFL-1 fibroblasts, or both, seeded in each well. The cells were fixed with 4% formaldehyde at RT for 15 min. The fixed cells were permeabilized with 0.5% Triton X-100 in phosphate-buffered saline (PBS), then blocked with a blocking buffer (1% bovine serum albumin/5% fetal bovine serum in PBS) at RT for 30 min before incubated with primary antibodies at 4 °C overnight. They were then incubated with a secondary antibody to detect the primary antibodies, followed by DAPI counterstaining. Cell images were visualized through confocal microscopy. More detailed information about the antibodies is provided in supplementary information (Table. S1).

2.8. Western blot

The cells were co-cultured in 6 well plates with GO-COL-coated glass coverslips. Approximately 1×10^5 THP-1 macrophages and 2×10^5 HFL-1 fibroblasts were co-cultured in each well for 24 h. Whole cell protein extracts were prepared with ice-cold RIPA lysis buffer supplemented with protease inhibitors, and quantified using a BCA protein assay kit (#23225, Thermo). Protein lysates were first isolated through 8% SDS-polyacrylamide gel electrophoresis (PAGE), and transferred to a polyvinylidene difluoride (PVDF) membrane (NEF1002, PerkinElmer). After blocking the membranes with 5% milk in TBST (0.1% Tween-20 in 1x TBS), the membranes were incubated overnight at 4 °C with primary antibodies diluted with 5% milk in TBST. After washing three times for 10 min each in TBST, the membranes were incubated with HRP-conjugated goat anti-rabbit/mouse IgG (H + L) secondary antibodies (#31460 and #31439, Thermo) for 1 h at RT. Finally, the membranes were incubated with ECL western blot substrate (WBKLS0500, Thermo Scientific) for 1 min, and images of the protein bands were captured using an imaging system.

2.9. Cell proliferation on GO-COL coated Titanium/Nitinol disks

The measurement of the CCK8 reagent is mentioned above. For proliferation tests, THP-1 and HFL-1 cells were co-cultured on GO-COL coated 12 mm Titanium/Nitinol disks with approximately 2×10^4 THP-1 macrophages and 4×10^4 HFL-1 fibroblasts, in a well. The optical density (OD) values were read on Day 1, Day 3, and Day 7. Statistical analysis and illustration were completed using Excel and Prism.

2.10. Measurement of pro-inflammatory cytokine expression

IL-6 and CCL2 expression levels were quantified using the Human IL-6 DuoSet ELISA kit (DY206–05, R&D) and Human CCL2/MCP-1 DuoSet ELISA kit (DY279–05, R&D). All the samples were assayed according to the manufacturer's instructions. The Coat Corning™ Costar™ 9018 ELISA plate wells were coated with capture antibodies overnight. Next, serial diluted standard and cell culture medium was transferred to each well of the ELISA plate. After incubation, the unbound conjugate was washed off, and detection antibodies were added to each well. After washing again, streptavidin-HRP was added to each well. Substrate was added to each well and incubated for 15 min, and the reaction was terminated using a stop solution (H_2SO_4). The OD in each well was measured at 450 nm using a microplate reader.

2.11. Measurement of pro-fibrotic cytokine expression

The activation of TGF-β in the cell culture experiments was measured using a TGFb1/LAP Human Uncoated ELISA Kit (Invitrogen, 88–50390). The Coat Corning™ Costar™ 9018 ELISA plate was incubated overnight at 4 °C with a capture antibody. After washing twice with wash buffer (0.05% Tween 20 in 1x PBS), the plate with 1x assay buffer was incubated at RT for 2 h. The plate was washed twice with 0.05% PBST, followed by loading of the plate with samples/standards. The detection antibody was then added to each well and incubated at RT for 2 h. After washing four times with 0.05% PBST, streptavidin-HRP was added, and the plate incubated at RT for 1 h. Finally, the plates were read at 450 nm using a microplate reader.

2.12. Statistical analysis

Each group of data was repeated at least three times, and the data are represented as the mean ± standard deviation. Statistical analysis was performed using GraphPad Prism (version 6) or Excel (Microsoft). The *t*-test for unpaired data was used for statistical analysis, and two-way analysis of variance was used for multiple comparisons.

3. Results and discussion

3.1. Fabrication and characterization of GO-COL composites

To synthesize the GO-COL composite, carboxylic groups present on the GO surface were first activated using 1-Ethyl-3-(3-dimethylaminopropyl) carbodiimide/N-hydroxysuccinimide (EDC/NHS) as cross-linking agents. Next, different concentrations of activated GO were made to react with the amine group on the COL to form covalent amide bonds (Fig. 1a). However, the electrostatic charges and Van der Waals forces generated between the GO nanosheets made them prone to agglomeration. During the synthesis of the GO-COL composites, excessive GO agglomerates were formed, affecting the synthesis efficiency and quality of the composite. Some parameters that can affect the dispersion of GO have been described, including pH, ionic strength, and temperature [31,32]; we synthesized GO-COL composites in an ice bath with ultrasound treatment in a chemical cross-linking reaction environment (Fig. S1).

Finally, GO-COL composites containing different weight percentages of GO (0%, 8%, 16%, and 32%; the composites are hereafter referred to as 8% GO-COL, 16% GO-COL, and 32% GO-COL) were prepared. In the C1s XPS spectrum, the GO-COL exhibited a higher C═O/C–NH (288.2 eV) peak than that exhibited by GO corresponding to the amide bonding formed in GO-COL, as shown in Fig. 1b. In addition, the spectra of N1s in GO-COL showed two additional N–H–C═O (400.4 eV) and N–H^{3+} (401.9 eV) peaks, which also proved the formation of more covalent bonds and hydrogen bonds in GO-COL (Fig. 1c). The chemical-bound composition of the GO-COL composites (Fig. 1d) was evident by Fourier-transform infrared spectroscopy (FTIR) showing absorption peaks appearing at C–N (1100–1300 cm^{-1}) and N–H (1560–1640 cm^{-1}). These results confirmed that the degree of cross-linking was higher in GO-COL composites compared to COL.

We subsequently analyzed the morphology of the GO-COL-coated substrates and found that the surface of the GO-COL coating became more textured as the weight percentage of GO in the GO-COL composite increased (Fig. 1e). The morphologies of the COL-and GO-COL-coated substrates were visualized by SEM imaging, and it was found that the GO-

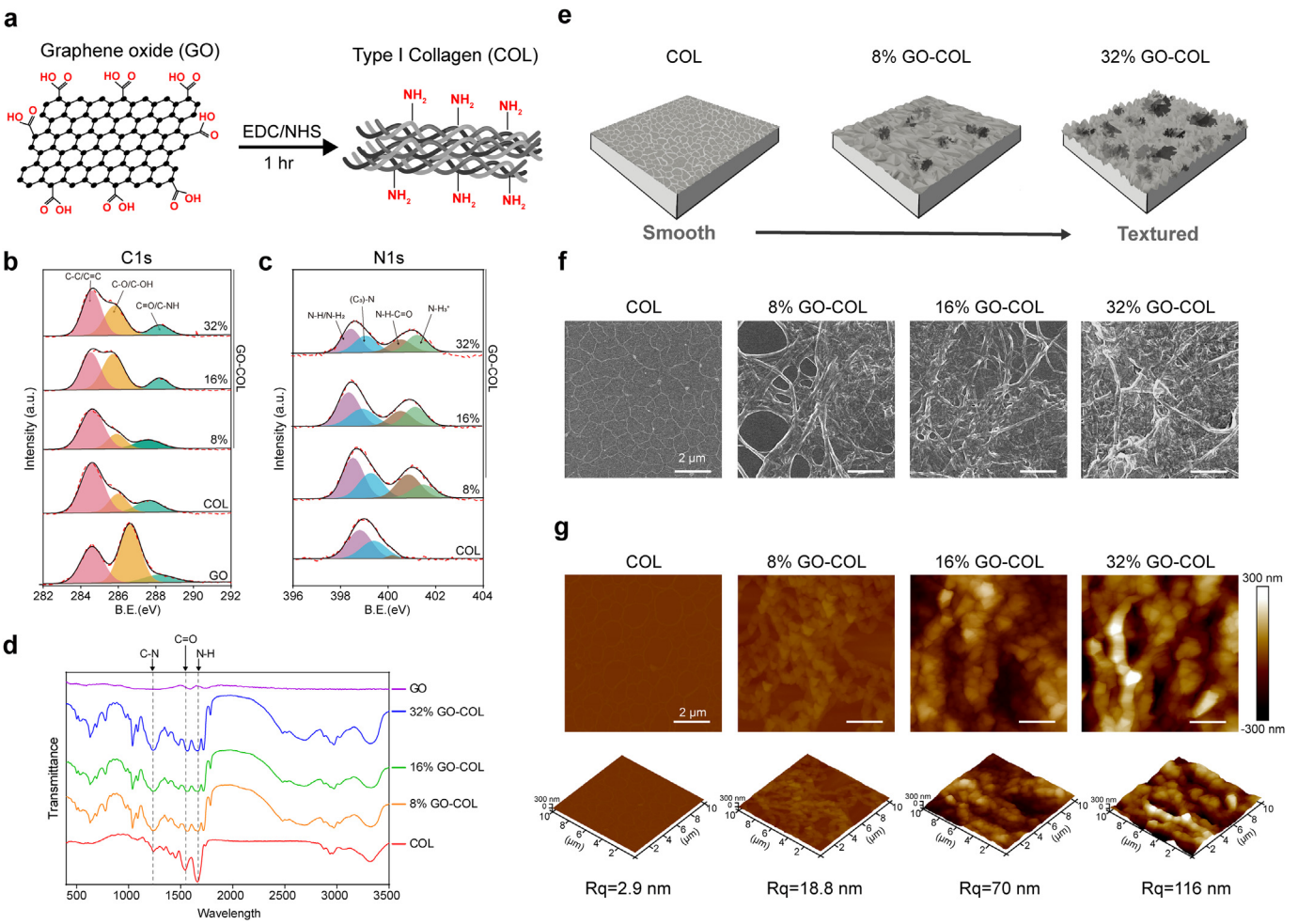

Fig. 1. Preparation and analysis of GO-COL biocompatible hybrid interface (a) Scheme of GO-COL conjugation. (b) XPS analysis of composites with different percentages of GO in interface. C1s spectra of GO, COL, 8% GO-COL, 16% GO-COL, and 32% GO-COL. GO-COL groups display a stronger C═O/C–NH (288.2 eV) bond than GO. (c) N1s spectra of COL, 8% GO-COL, 16% GO-COL, and 32% GO-COL where GO-COL presents stronger N–C═O (399.8 eV) and C–NH^{3+} (401.4 eV) binding energy than COL. (d) FTIR spectra of COL, 8% GO-COL, 16% GO-COL, 32% GO-COL, and GO are measured and illustrated. Peaks are characterized at different wavelengths, C = O (1650 nm-1), N–H (1560–1640 cm-1), and C–N (1100–1300 cm-1). (e) Scheme of changes in structure of regulating GO at different concentrations. (f) SEM image at different percentages of GO-COL coating surface. (g) AFM analysis at different percentages of GO-COL topography.

COL formed a three dimensional (3D) cross-linking network structure, whereas COL formed a two dimensional (2D) mesh structure (Fig. 1f). These structural differences stem from the addition of GO, which contributed to tighter connections among the separated nanoscale fibrous structures in the GO-COL composites. GO facilitates the structural alignment of COL fibers through supramolecular interactions, including hydrogen bonding, electrostatic interactions, and π-π stacking [33]. In addition, the amide bond formed between GO and COL further enhances the cross-linking effect, resulting in the formation of a 3D network structure of GO-COL [34]. Analysis of the surface topography showed that the roughness increased with increasing GO concentration, as shown in Fig. 1e. The COL showed a root mean square (RMS) roughness of 2.9 nm. As for GO-COL, the addition of GO resulted in an increase in RMS roughness from 18.8 nm to 116 nm for 8% GO-COL and 32% GO-COL respectively. In addition, the higher GO concentration in GO-COL composites also increased the stiffness to 19.26 kPa on the GO-COL composite with a GO weight percentage of 32%. (Fig. S2). In comparison, COL was softer than GO-COL and had a stiffness of 5.87 kPa. Considering these factors, we incorporated GO into COL, creating a 3D fibrous structure with nanoscale roughness that simultaneously enhanced material stiffness.

Other studies on GO-incorporated hydrogels also reported that different ways of cross-linking GO sheets improved mechanical properties such as stiffness, dimensionality, surface roughness, porosity, and deformability [35,36]. The hydrogels were designed to create various degrees of mechanical strength that regulate cell behavior, which provided researchers with a biomaterial platform for modeling *in vitro* cell research and tissue engineering applications [27,29,37]. Here, we focus on how GO-COL coatings influence the phenotypic changes of fibroblasts and macrophage cells, and assess the feasibility of their use in anti-fibrotic applications.

3.2. Fibroblast cell morphology on GO-COL coatings

It has been well documented that quiescent fibroblasts are activated to transform into myofibroblasts during the tissue healing process. This leads to cytoskeletal structural alterations and alpha-smooth muscle actin (α-SMA) expression through the activation of the focal adhesion kinase (FAK) pathway [38,39]. Myofibroblasts are responsible for enhancing the secretion of ECM and thus repairing injured tissue. However, continued activation of the myofibroblasts can also lead to cell proliferation, resulting in the accumulation of abnormal ECM and altered tissue mechanical properties, eventually leading to fibrosis [6]. Therefore, a balanced activation of fibroblasts is important for reducing fibrotic capsule formation during the wound healing process.

To demonstrate the applicability and effectiveness of GO-COL as an

anti-fibrotic coating, we studied the cell morphology and myofibroblast marker (α-SMA) expression in HFL-1 fibroblasts seeded on GO-COL to analyze their differentiation levels (Fig. 2a). Fibroblasts were cultured on the GO-COL coating for 24 h, and cell viability was examined by the CCK8 assay. As shown in Figs. 2b and 8% GO-COL, 16% GO-COL, and 32% GO-COL did not show significant differences in cell viability compared to COL, demonstrating the biocompatibility of the GO-COL coatings. The cell morphology of myofibroblasts usually exhibits a spreading shape similar to that of quiescent fibroblasts [40]. We examined fibroblast morphology using the mesenchymal marker-vimentin. Cells on GO-COL showed lower vimentin expression, which we speculated was due to the decrease in cell aspect ratio and cell area (Fig. 2c and d). To further confirm and analyze the influence of myofibroblast differentiation on the GO-COL coatings, the cells were immunostained with the myofibroblast marker α-SMA. Confocal images (Fig. 2c) showed that HFL-1 fibroblasts grown on COL expressed more α-SMA filaments, while fibroblasts grown on the 8% GO-COL, 16% GO-COL, and 32% GO-COL indicated a GO concentration-dependent decrease (Fig. 2e). According to previous studies, stiff substrates promote the formation of stress fibers and α-SMA expression in myofibroblasts [41,42]. Since COL only formed a mesh-like 2D structure on the glass surface, the cells cultured on the COL-coated coverslips were still affected by the stress of the glass substrate, leading to myofibroblast activation. High matrix stiffness triggers the mechanosensitive Hippo pathway effector Yes-associated protein 1 (YAP) [43]. Conversely, activated YAP upregulates myofibroblast differentiation, resulting in increased ECM deposition and tissue stiffness [44]. Excessive deposition of ECM establishes an aggressive pro-fibrotic feedback loop, which stimulates fibrotic tissue proliferation [45]. In contrast, GO-COL composites form a 3D fibrous structure that creates a softer matrix between the cells and the glass, maintaining the quiescent phenotypic nature of the fibroblasts. In addition, the topological nanostructure of the surface also played an important role in inhibiting the differentiation of fibroblasts into myofibroblasts [46]. The cross-linking of GO with COL, forming anisotropic fibers, can potentially regulate the expression of α-SMA in fibroblasts, as observed in previous studies [47]. Topologically anisotropic fibrillar microstructure inhibits the

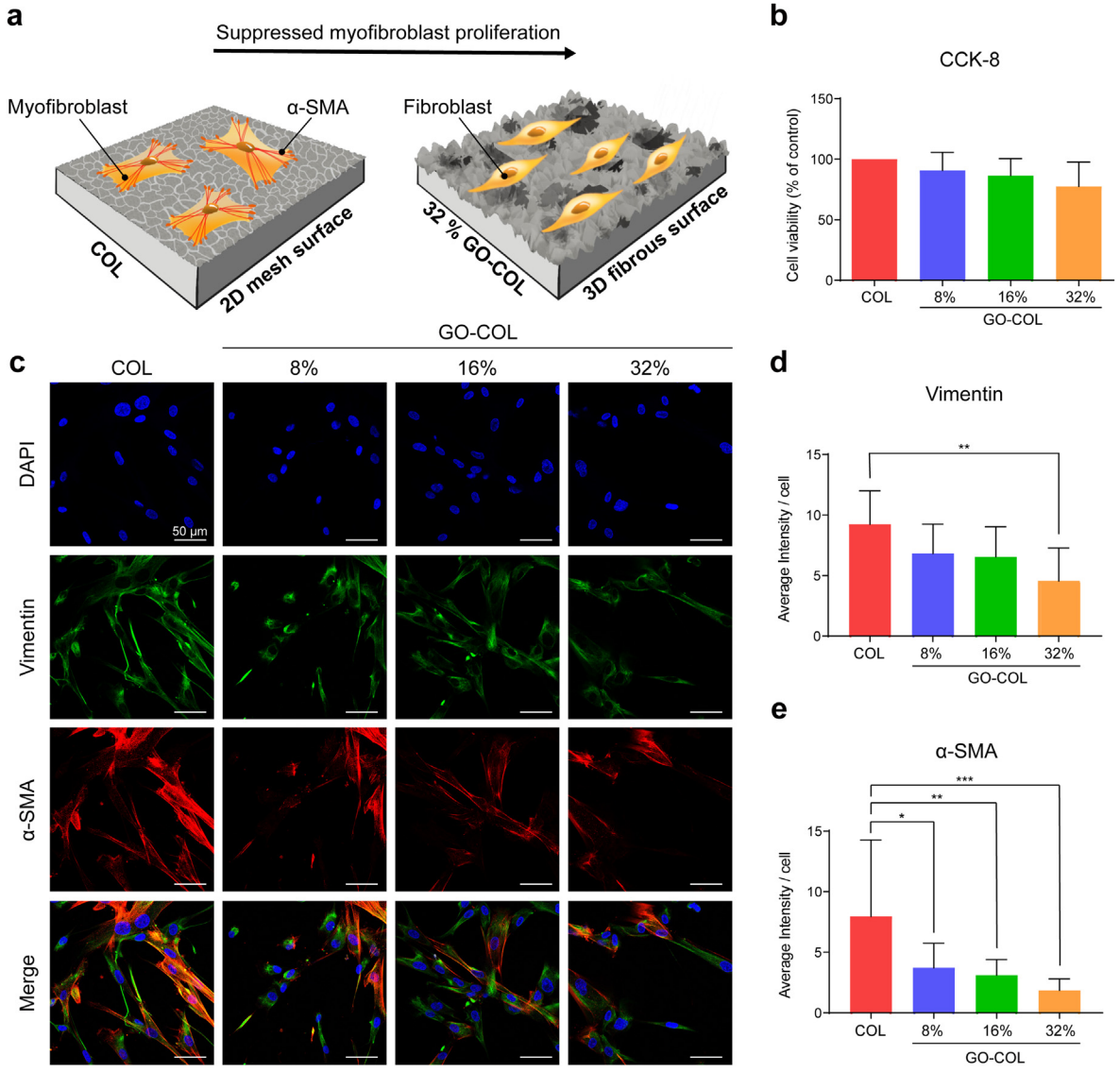

Fig. 2. Response of HFL-1 fibroblast cultured on GO-COL biocompatible hybrid interface. (a) Scheme of fibroblast and myofibroblast morphology changes on COL and GO-COL. (b) Viability of cells cultured for 24 h. (c) Immunofluorescence images of cells cultured on COL, 8% GO-COL, 16% GO-COL, and 32% GO-COL. HFL-1 fibroblasts demonstrate higher myofibroblast marker α-SMA expression levels on COL compared to GO-COL; α-SMA expression levels show decreasing trends with increasing GO percentage in GO-COL, with 32% group presenting least α-SMA areas. (d) Quantification of vimentin expression areas. (e) Quantification of α-SMA expression areas among COL, 8% GO-COL, 16% GO-COL, and 32% GO-COL. Statistics are normalized based on COL. HFL-1 cells on 32% GO-COL show least α-SMA expression, presenting the best anti-fibrotic capability among all GO-COL groups.

activation of integrin β1 ligands on fibroblasts and further suppresses the YAP signaling involved in α-SMA-mediated fibrosis [45].

3.3. Polarization of macrophages on GO-COL coatings

Macrophages play a key regulatory role in wound healing and maintaining pro-fibrotic environments [48]. Each macrophage phenotype plays a unique and critical role in different stages of tissue repair; therefore, the dynamic regulation of macrophage subtypes and their functions is important. Specific environmental factors can polarize macrophages from the ground state M0 into two major subtypes: the pro-inflammatory M1 type and the M2 type in which tissue repair is promoted [49]. Although both pro- and anti-inflammatory macrophages are indispensable for regular tissue repair, overactivation of either subpopulation is undesirable. M1 macrophages are involved in angiogenesis and phagocytosis during early wound healing, but an overly intense M1 inflammatory response leads to tissue destruction and fibrosis. Similarly, although M2 macrophages promote tissue repair, an overabundance of M2 macrophages might cause high expression of TGF-β, and enhance fibrotic capsule formation. Therefore, the state of balance of the M1/M2 ratio is an important factor that determines the success or failure of bio-implants [50].

To clarify the propensity of the macrophages for polarization on the GO-COL coating, THP-1 monocytes were first seeded on GO-COL coatings; the suspension-type THP-1 monocytes were then treated with propidium monoazide (PMA) for them to differentiate into an adhesive macrophage-like phenotype. A PMA concentration of 150 nM and treatment time of 6 h were provided, based on past researches [51,52]. After 6 h of incubation, the THP-1 cells that were attached to the GO-COL had transformed into a macrophage-like phenotype. As a comparison, we also induced the transformation of THP-1 macrophages into an M1 positive phenotype using interferon-γ (IFN-γ) and lipopolysaccharide (LPS). After 24 h of culture, the cells were immunostained with the CD163 antibody. CD163 markers were found in M0, M1, and M2 macrophages, but the M2 macrophages showed increased expression. Confocal images (Fig. 3a) showed decreased expression of CD163 in the M1 positive COL (IFN-γ+/LPS+) group and M0 THP-1 macrophages seeded on the GO-COL, compared to macrophages seeded on COL. In addition, GO-COL showed a decreasing trend of CD163 expression as the GO content in the composite increased. Flow cytometry was used for further quantification of the fluorescent expression of CD163 on THP-1 macrophages (Fig. 3b). Macrophages seeded on the 32% GO-COL

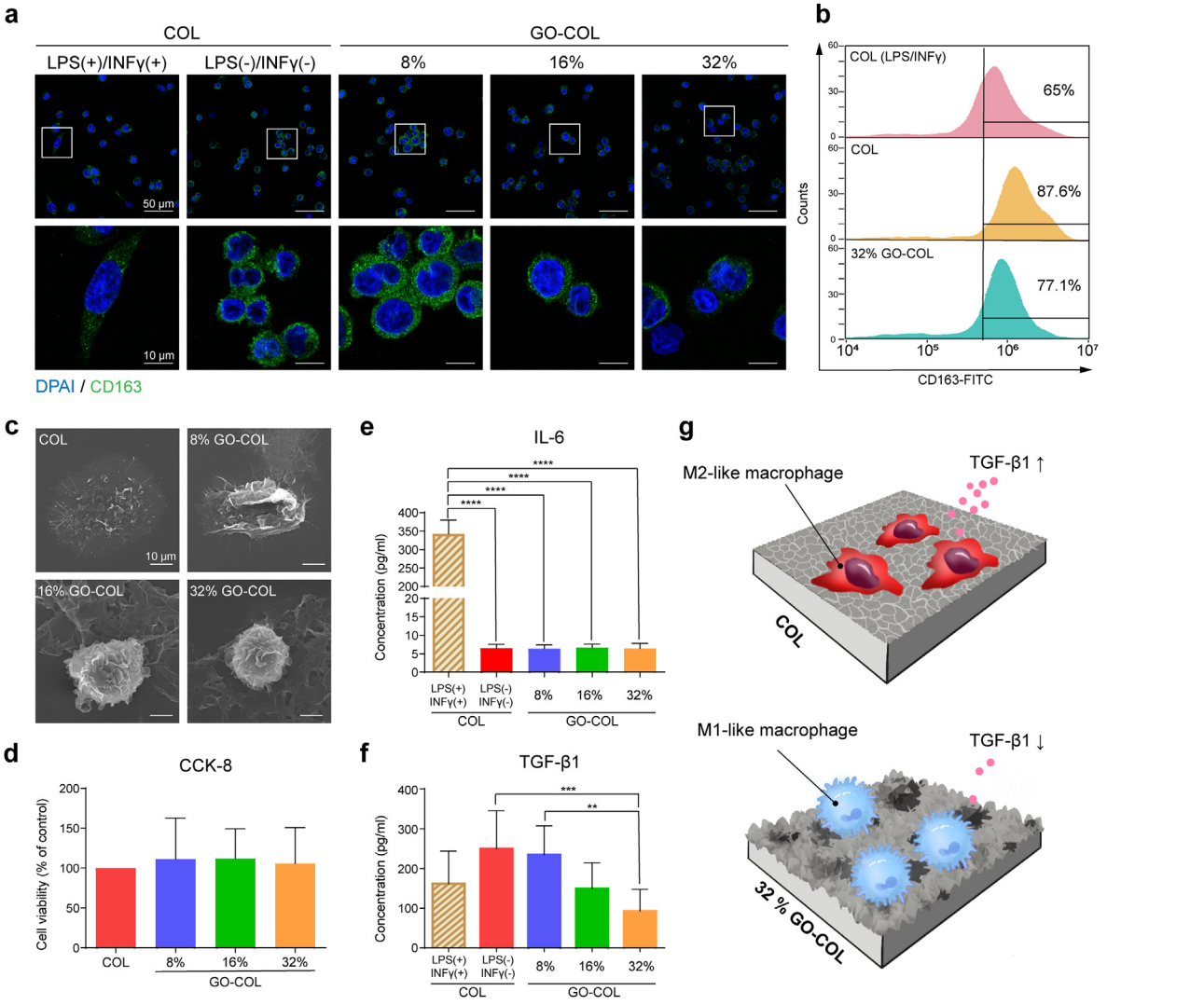

Fig. 3. THP-1 Macrophage polarization on GO-COL biocompatible hybrid interface. (a) Immunofluorescence images of M2 macrophage marker CD163 of COL, COL with IFN-γ/LPS treatment, 8% GO-COL, 16% GO-COL, and 32% GO-COL. (b) Flow cytometry analysis of CD163 marker fluorescence intensity (MFI) among COL, COL with IFN-γ/LPS treatment, and 32% GO-COL. (c) SEM images of morphology of THP-1 macrophage on GO-COL. (d) Viability of THP-1 macrophage cultured for 24 h. (e–f) Expression of fibrosis related cytokines in THP-1 macrophages on GO-COL. ELISA analysis of TGF-β1 and IL-6 concentration among COL, COL with IFN-γ/LPS treatment, 8% GO-COL, 16% GO-COL, and 32% GO-COL. (g) Scheme of THP-1 macrophages cultured on COL and GO-COL coating surface.

showed a 10% downregulation in CD163 expression compared to macrophages seeded on COL. Furthermore, CD163 expression in macrophages seeded on 32% GO-COL was increased by 12% compared to that on the M1 positive COL (IFN-γ+/LPS+) group. We also analyzed M1 markers (TLR2 and CCR7) and found that THP-1 macrophages on GO-COL showed higher M1 marker expression than cells seeded on COL (Fig. S3). These results suggested that GO-COL inhibited the differentiation of macrophages into M2 macrophages, with 32% GO-COL possessing the greatest inhibition capability among all the GO concentrations considered.

The macrophage subtypes were also quite different in morphology. We observed the detailed surface morphology of THP-1 macrophages using SEM images. As shown in Fig. 3c, THP-1 macrophages exhibited a flatter morphology on COL, with fewer membrane wrinkles seen on the cell surface, similar to the M2 phenotype of human macrophages [53]. In contrast, THP-1 macrophages seeded on the GO-COL coatings were more spherical and exhibited more membrane folds, showing more similarity to the morphology of M0/M1 macrophages. The biocompatibility of THP-1 macrophages cultured on GO-COL was confirmed using the CCK8 assay (Fig. 3d).

GO has been reported to interact with cell membranes, thereby altering the phenotype and function of macrophages. For example, GO nanosheets can activate toll-like receptors (TLRs) of macrophages through multivalent interactions between the functionalized surface and TLRs on the cell membrane, and activated TLRs promote macrophage M1 polarization through typical NF-κB signaling [25,54]. Moreover, GO carbon radicals trigger surface oxidation that causes lipid peroxidation in macrophage membranes, resulting in phenotypic and functional changes [22]. According to our findings, the GO-COL coating induced THP-1 macrophages to transform into the M1-like phenotype as the concentration of GO increased. Interestingly, THP-1 macrophages induced by GO-COL did not produce excessive amounts of the pro-inflammatory factor -Interleukin-6 (IL-6) compared to those induced by IFN-γ and LPS (Fig. 3e). However, previous studies have observed that stimulation with GO nanosheets resulted in high levels of pro-inflammatory factor secretion by macrophages [55]. Li et al. have found that oxygen functional groups level and carbon radicals density on the GO surface may determine its toxicity [56]. The OH, COOH, and COC groups on the GO surface in contact with the cell membrane may oxidize unsaturated lipids [57]. Lipid peroxidation can lead to failure of membrane integrity, which in turn induces significantly higher levels of pro-inflammatory cytokines. We speculated that due to the tight cross-linking of GO-COL composites,

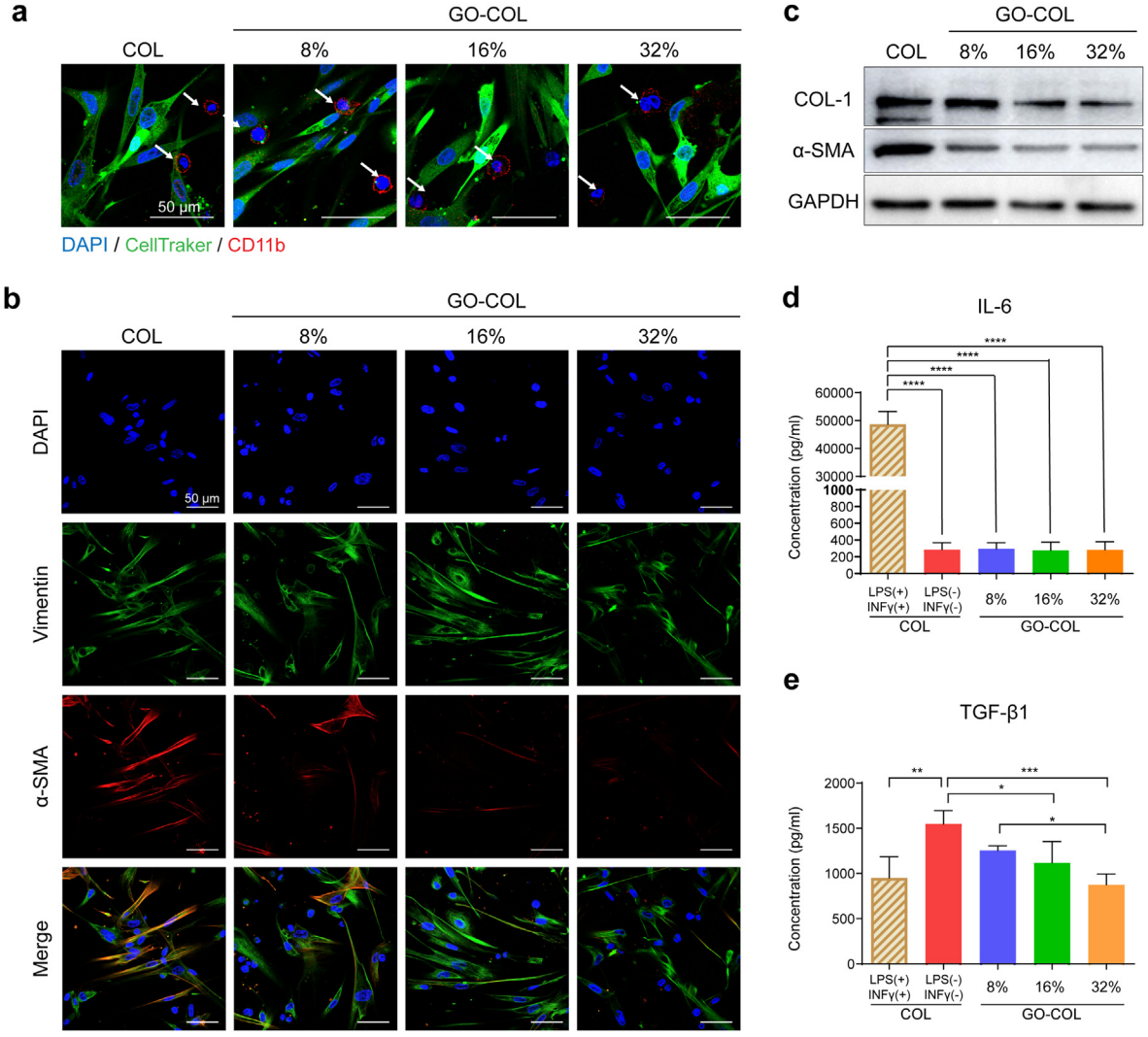

Fig. 4. Co-culture of Fibroblast/Macrophage on GO-COL biocompatible hybrid interface. (a) Immunofluorescence images of co-culturing THP-1 macrophages and HFL-1 fibroblasts. HFL-1 fibroblasts are labeled with green tracking dye, and THP-1 macrophages are stained with macrophage specific marker CD11b. (b) Immunofluorescence images of THP-1 macrophages/HFL-1 fibroblasts co-cultured on COL, 8% GO-COL, 16% GO-COL, and 32% GO-COL. GO-COL groups show less α-SMA expression levels compared to COL. (c) Result of western blot of 24 h co-culture. (d–e) ELISA analysis of TGF-β1 and IL-6 concentrations among COL, COL with IFN-γ/LPS treatment, 8% GO-COL, 16% GO-COL, and 32% GO-COL.

the interaction of GO with cell membranes decreased, lowering the differentiation of pro-inflammatory M1 types, while GO-COL also inhibited the differentiation of M2 macrophages and reduced the secretion of TGF-β1 (Fig. 3f). TGF-β1, being a potent pro-fibrotic cytokine, mediates fibrosis and induces differentiation into myofibroblasts. Altogether, the nanoscale roughness of GO-COL, coupled with the oxygen functional groups on GO, synergistically influenced the polarization of macrophages (Fig. 3g).

3.4. Anti-fibrotic attributes of GO-COL coatings under pro-fibrotic environments

Fibroblast-macrophage interactions affect tissue repair, regeneration, and fibrosis after implantation [7]. To further investigate the ability of the GO-COL coating to inhibit fibrosis under conditions of fibroblast-macrophage interactions, we first created a macrophage and fibroblast co-culture model by seeding THP-1 cells on coated coverslips and treating them with PMA to induce macrophage-like differentiation. Next, HFL-1 fibroblasts were seeded and co-cultured with the macrophages for 24 h. We labeled HFL-1 with tracking dye, and immunostained THP-1 with the macrophage marker CD11b to verify the successful co-culture of fibroblasts and macrophages on COL and GO-COL coatings (Fig. 4a). The ratio of fibroblasts to macrophages affects the level of fibrosis through cell-cell interactions [58]. To observe the ability of the GO-COL coating to inhibit fibrosis in a highly fibrotic co-culture model, we set the ratio of the number of macrophage cells and co-cultured fibroblast cells to different values (fibroblast/macrophage ratios of 2:1, 4:1, 8:1, and 16:1), followed by immunostaining with the α-SMA marker to confirm the differentiation of myofibroblasts on COL-coated coverslips. As shown in Supplementary (Fig. S4), statistical results did not indicate significant differences among the α-SMA expression levels in each group (2:1, 4:1, 8:1, and 16:1) However, the 2:1 ratio showed a higher level of fibrosis; therefore, it was selected as the best co-culture ratio for studying the anti-fibrotic ability of the GO-COL coating.

The anti-fibrotic ability of the GO-COL coating was examined by immunostaining HFL-1 fibroblasts with myofibroblast markers (α-SMA) in a pro-fibrotic environment within a fibroblast/macrophage co-culture model. The results showed that the α-SMA marker in the HFL-1 tended to decrease with increasing GO concentration in the GO-COL composite (Fig. 4b). COL-I is also considered a fibrosis marker because, when fibroblasts differentiate into myofibroblasts, it is overproduced and deposited, creating a stiff ECM [59]. Therefore, we collected cell lysates from 24 h co-cultures and analyzed them with western blot for more accurate quantification. As shown in Fig. 4c, the results of the western blot showed that the GO-COL coating inhibited the expression of α-SMA and COL-I in HFL-1 fibroblasts. In the GO-COL-coated group, secretion of the fibrosis-associated cytokine TGF-β1 was significantly reduced (Fig. 4d), and the inflammatory mediator IL-6 showed no significant increase (Fig. 4e). These results indicate that the GO-COL coating did not trigger a strong inflammatory response under conditions of fibroblast-macrophage interaction, and could inhibit myofibroblast differentiation. These results are consistent with the research of Li et al. who demonstrated that GO-COL hybrid membranes reduced gene expression associated with fibrosis, collagen metabolism, and scar formation [60]. The GO-COL hybrid membrane also showed less neutrophil and macrophage accumulation and a lower inflammatory response in the healing area compared to COL membrane. These demonstrate the potential of GO-COL for anti-fibrotic applications.

Fibrosis is a progressive disease that becomes aggressive over time. To study whether the inhibition of myofibroblast differentiation by the GO-COL coating is sustainable, we further examined the expression of α-SMA markers of HFL-1 at days 3 and 7. As shown in Fig. S5, although the expression of α-SMA increased with time for all groups, the HFL-1 on the GO-COL coating showed a 75% decrease in the a-SMA expression at day 7 compared to the uncoated group, while the HFL-1 on COL showed only a 31% decrease. This result demonstrated the anti-fibrotic potential of the GO-COL coating in the pro-fibrotic environment within 7 days. Fibroblasts with high expression of α-SMA markers indicate a pro-fibrotic myofibroblast phenotype, which is an important pathological feature of pre-fibrosis.

3.5. Application of GO-COL coatings on implants

The long-term stability of implants is often limited by FBRs, especially in metallic implants [61]. It is well known that most metals are not bioactive, which causes the accumulation of M1 macrophages and induces acute and chronic inflammatory responses [62]. On the other hand, high surface mechanical stress induces excessive differentiation of myofibroblasts, leading to the formation of fibrotic tissues such as scars and granulomas [63,64]. To further clarify the potential of the GO-COL coating for metal implants, we coated the COL and the GO-COL composites on titanium and nitinol disks (Fig. S6) and analyzed the markers of inflammation and fibrosis using a fibroblast/macrophage co-culture model. First, COL-I was labeled by immunofluorescence staining with Alexa-488 conjugated secondary antibodies to confirm COL and GO-COL coating on the disks. As shown in Fig. 5a, the region with green fluorescent signal appeared in both the COL and GO-COL groups. Notably, the arrangement of COL-I fibers on the GO-COL coated surface was more dispersed than on the COL coated surface, which was attributed to the difference in nanostructures and mechanical properties between GO-COL and COL. We had confirmed the difference in nanostructures (3D fibrous versus 2D planar) and mechanical properties between GO-COL and COL.

Next, we set up the macrophage and fibroblast co-culture model described previously for titanium and nitinol disks, with and without COL and GO-COL coatings. Cell proliferation was analyzed using the CCK8 assay on days 1, 3, and 7 (Fig. 5b). The results showed that the GO-COL-coated and COL-coated groups maintained similar cell proliferation rates on titanium disks for one week. However, cells on nitinol disks—with or without COL and GO-COL coatings—showed a low cell proliferation rate. Other studies have indicated the possible dissolution of nickel from nitinol to form nickel ions in solution, decreasing cell proliferation or inhibiting cell growth on the substrate. To confirm whether titanium and nitinol coated with the GO-COL composite could reduce myofibroblast differentiation, we also checked the expression of α-SMA markers of HFL-1 by immunofluorescence staining on days 1, 3, and 7. The results showed that HFL-1 on the GO-COL-coated titanium and nitinol groups exhibited a smaller increase in levels of α-SMA expression than the COL-coated and uncoated groups over time (Fig. 5c). The confocal fluorescence images showed that the cells grown on titanium and nitinol disks exhibited elongated and highly oriented morphology (Fig. 5d and e). Such cell morphology was observed because cells tend to grow along the grooves caused by the grinding process, and therefore, the contact micro-grooves induced cell alignment and migration [65]. The GO-COL coating created nanoscale fibrous structures on the micro-grooves, reducing the differentiation of pro-fibrotic myofibroblasts while maintaining cell growth. After 7 days of immersion in the medium, the GO-COL coating on titanium and nitinol discs still held the 3D fibrous structure (Fig. S7). In addition, the fibrosis-associated cytokine TGF-β1 was reduced in the GO-COL-coated group compared to the COL-coated groups (Fig. 5f). By day 7, TGF-β1 protein expression increased compared to that on day 1, probably due to cell proliferation.

The continuous release of chemokines, cytokines, and other mediators promotes the formation of an inflammatory microenvironment, which eventually affects tissue remodeling at the site surrounding the implant [66,67]. The inflammatory mediator IL-6 showed no significant increase after 7 days (Fig. 5g) in the COL-or GO-COL-coated titanium and nitinol groups. In addition, we analyzed chemokine ligand 2 (CCL-2), an important regulatory molecule for the recruitment of macrophages to the implant; the results showed no significant increase after 7 days (Fig. 5h). Our findings suggested that GO-COL-coated titanium and nitinol have the potential to modulate the excessive release of pro-inflammatory factors from co-cultured fibroblasts and macrophages.

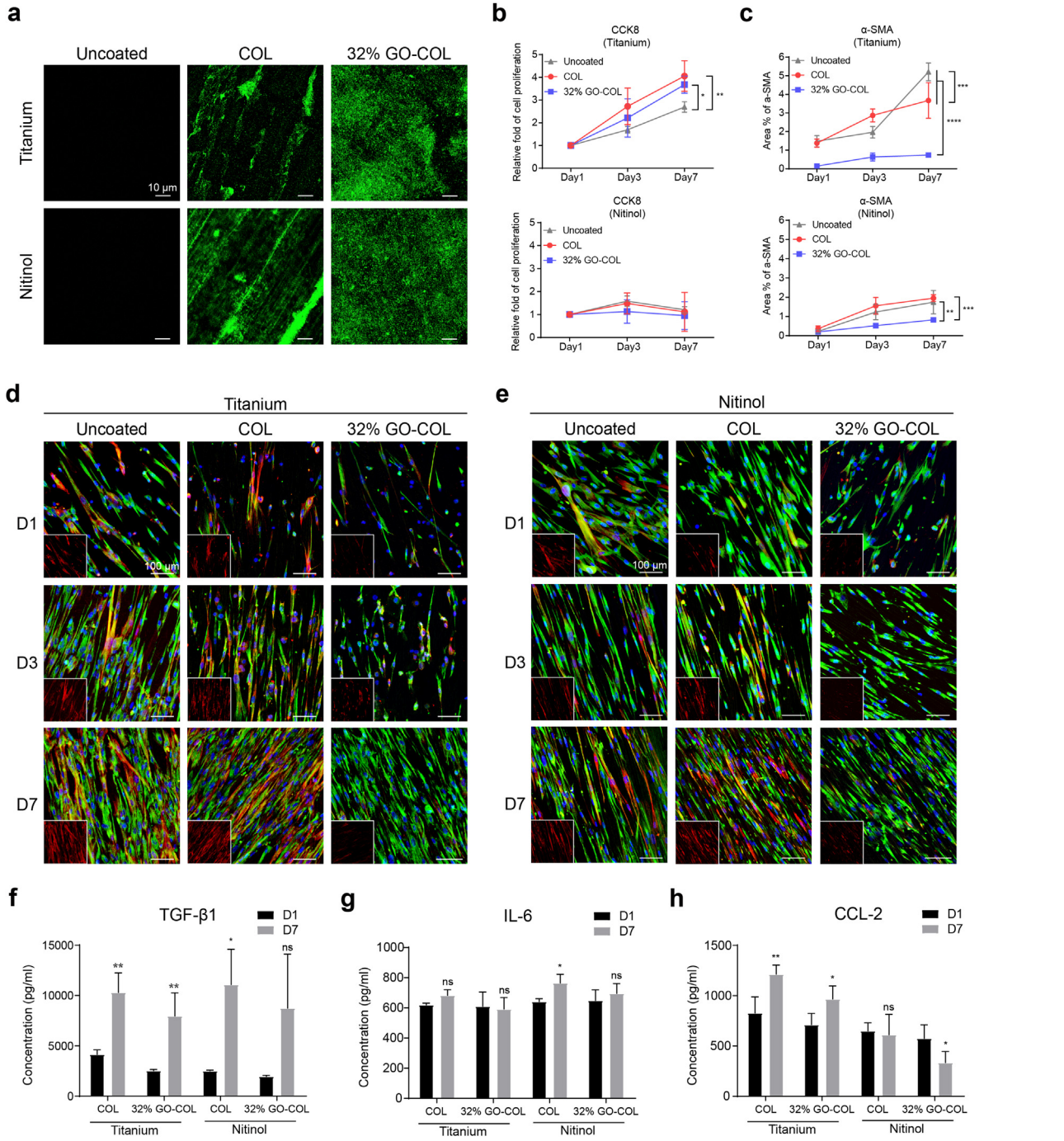

Fig. 5. Performance of biohybrid interface coated on Titanium/Nitinol disk. (a) Immunofluorescence staining of COL-I on uncoated, COL coated, and 32% GO-COL coated surfaces. (b) Cell proliferation and (c) quantification of α-SMA expression on uncoated, and COL and 32% GO-COL coated Titanium disks from Day 1 to Day 7. (d) Immunofluorescence images of fibroblasts and macrophages co-cultured on uncoated, and COL, and 32% GO-COL coated surfaces at Day 1, Day 3, and Day 7. Myofibroblast marker α-SMA is stained with Cy3, labeled in red. Mesenchymal marker vimentin is labeled in green. (e) Immunofluorescence images of fibroblasts and macrophages co-cultured on different surfaces on Nitinol. Myofibroblast marker α-SMA is labeled in red and vimentin is labeled in green. ELISA test of (f) TGF-β1, (g) IL-6 and (h) CCL-2 cytokine expressions of cells on COL and 32% GO-COL coated Titanium/Nitinol disks.

4. Conclusions

In this study, a novel biocompatible hybrid interface was developed to reduce FBRs and incidence of fibrotic capsules. It was demonstrated that the GO-COL interface generates unique surface nanostructures by providing nano roughness to inhibit myofibroblast differentiation. Moreover, this interface decreased M2 macrophage polarization and limited the production of more pro-inflammatory factors. This avoids the bottleneck arising from the use of a nano interface that induces a strong immune response. In addition, the expressions of fibrosis-related proteins α-SMA and collagen-reduced significantly when fibroblasts and macrophages were co-cultured on GO-COL. Collectively, our results demonstrated that GO-COL provides definite advantages over GO or ECM alone in modulating cell interactions between fibroblasts and macrophages, and are anti-fibrotic when applied onto common metallic implants, titanium and nitinol. The GO-COL bio-interface thus demonstrates potential as a new therapeutic strategy against implant fibrosis through an immunomodulatory concept that had remained underestimated so far.

Credit author statement

C.-Y.C. and P.-H.T. contributed equally to this work. C.-Y.C. and P.-H.T.: Conceptualization, Methodology, Validation, Visualization, Investigation, and Writing – original draft. Y.-H.L.: Conceptualization, Methodology, and Investigation. C.-Y.H.: Resources and Writing – review & editing. J.H.Y.C.: Resources and Writing – review & editing. G.-Y.C.: Conceptualization, Funding acquisition, Supervision and Writing – review & editing.

Data and materials availability

All data needed to support the conclusions are present in the paper and/or the Supplementary Materials. Additional data related to this paper may be requested from the authors.

Declaration of competing interest

The authors declare that they have no known competing financial interests or personal relationships that could have appeared to influence the work reported in this paper.

Acknowledgments

G.-Y.C. would like to acknowledge funding from the Ministry of Science and Technology (MOST111-2636-E-A49-005-), Council of Agriculture, Executive Yuan (111AS-13.2.1-AD-U2) and the Higher Education Sprout Project of the National Yang Ming Chiao Tung University and Ministry of Education (111W20211, 111W20271), Taiwan. J.H.Y.C would like to acknowledge funding from the Australian National Fabrication Facility (ANFF) materials node.

Appendix A. Supplementary data

Supplementary data to this article can be found online at https://doi.org/10.1016/j.mtbio.2022.100326.

References

[1] D. Zhang, Q. Chen, C. Shi, M. Chen, K. Ma, J. Wan, R. Liu, Dealing with the foreign-body response to implanted biomaterials: strategies and applications of new materials, Adv. Funct. Mater. 31 (6) (2021), 2007226.
[2] M. Kastellorizios, N. Tipnis, D.J. Burgess, Foreign Body Reaction to Subcutaneous Implants, Immune Responses to Biosurfaces, 2015, pp. 93–108.
[3] A. Carnicer-Lombarte, S.-T. Chen, G.G. Malliaras, D.G. Barone, Foreign body reaction to implanted biomaterials and its impact in nerve neuroprosthetics, Front. Bioeng. Biotechnol. (2021) 271.
[4] A. Boddupalli, L. Zhu, K.M. Bratlie, Methods for implant acceptance and wound healing: material selection and implant location modulate macrophage and fibroblast phenotypes, Adv. Health. Mater. 5 (20) (2016) 2575–2594.
[5] J.M. Anderson, A. Rodriguez, D.T. Chang, Foreign body reaction to biomaterials, Semin. Immunol. 20 (2) (2008) 86–100.
[6] P. Pakshir, B. Hinz, The big five in fibrosis: macrophages, myofibroblasts, matrix, mechanics, and miscommunication, Matrix Biol. 68–69 (2018) 81–93.
[7] C.E. Witherel, D. Abebayehu, T.H. Barker, K.L. Spiller, Macrophage and fibroblast interactions in biomaterial-mediated fibrosis, Adv. Health. Mater. 8 (4) (2019), 1801451.
[8] S. Mukherjee, S. Darzi, K. Paul, J.A. Werkmeister, C.E. Gargett, Mesenchymal stem cell-based bioengineered constructs: foreign body response, cross-talk with macrophages and impact of biomaterial design strategies for pelvic floor disorders, Interface Focus 9 (4) (2019) 15.
[9] B.N. Brown, S.F. Badylak, Expanded applications, shifting paradigms and an improved understanding of host-biomaterial interactions, Acta Biomater. 9 (2) (2013) 4948–4955.
[10] C. Li, C. Guo, V. Fitzpatrick, A. Ibrahim, M.J. Zwierstra, P. Hanna, A. Lechtig, A. Nazarian, S.J. Lin, D.L. Kaplan, Design of biodegradable, implantable devices towards clinical translation, Nat. Rev. Mater. 5 (1) (2019) 61–81.
[11] H.S. Dhowre, S. Rajput, N.A. Russell, M. Zelzer, Responsive cell–material interfaces, Nanomedicine 10 (5) (2015) 849–871.
[12] B. Ulmasov, B.A. Neuschwander-Tetri, J. Lai, V. Monastyrskiy, T. Bhat, M.P. Yates, J. Oliva, M.J. Prinsen, P.G. Ruminski, D.W. Griggs, Inhibitors of Arg-Gly-Asp-binding integrins reduce development of pancreatic fibrosis in mice, Cell. Mol. Gastroenterol. Hepatol. 2 (4) (2016) 499–518.
[13] N. Noskovicova, B. Hinz, P. Pakshir, Implant fibrosis and the underappreciated role of myofibroblasts in the foreign body reaction, Cells 10 (7) (2021).
[14] H. Majd, S.S. Scherer, S. Boo, S. Ramondetti, E. Cambridge, W. Raffoul, M. Friedrich, B. Pittet, D. Pioletti, B. Hinz, G. Pietramaggiori, Novel micropatterns mechanically control fibrotic reactions at the surface of silicone implants, Biomaterials 54 (2015) 136–147.
[15] J. Padmanabhan, E.R. Kinser, M.A. Stalter, C. Duncan-Lewis, J.L. Balestrini, A.J. Sawyer, J. Schroers, T.R. Kyriakides, Engineering cellular response using nanopatterned bulk metallic glass, ACS Nano 8 (5) (2014) 4366–4375.
[16] J. Kim, H.N. Kim, K.T. Lim, Y. Kim, H. Seonwoo, S.H. Park, H.J. Lim, D.H. Kim, K.Y. Suh, P.H. Choung, Y.H. Choung, J.H. Chung, Designing nanotopographical density of extracellular matrix for controlled morphology and function of human mesenchymal stem cells, Sci. Rep. 3 (2013) 3552.
[17] K.B. Narayanan, G.T. Park, S.S. Han, Electrospun poly(vinyl alcohol)/reduced graphene oxide nanofibrous scaffolds for skin tissue engineering, Colloids Surf. B Biointerfaces 191 (2020), 110994.
[18] Y.C. Shin, K.M. Pang, D.W. Han, K.H. Lee, Y.C. Ha, J.W. Park, B. Kim, D. Kim, J.H. Lee, Enhanced osteogenic differentiation of human mesenchymal stem cells on Ti surfaces with electrochemical nanopattern formation, Mater Sci Eng C Mater Biol Appl 99 (2019) 1174–1181.
[19] F. Robotti, S. Bottan, F. Fraschetti, A. Mallone, G. Pellegrini, N. Lindenblatt, C. Starck, V. Falk, D. Poulikakos, A. Ferrari, A micron-scale surface topography design reducing cell adhesion to implanted materials, Sci. Rep. 8 (1) (2018), 10887.
[20] S. Gurunathan, J.H. Kim, Synthesis, toxicity, biocompatibility, and biomedical applications of graphene and graphene-related materials, Int. J. Nanomed. 11 (2016) 1927–1945.
[21] J.J. Grant, S.C. Pillai, S. Hehir, M. McAfee, A. Breen, Biomedical applications of electrospun graphene oxide, ACS Biomater. Sci. Eng. 7 (4) (2021) 1278–1301.
[22] R. Li, L.M. Guiney, C.H. Chang, N.D. Mansukhani, Z. Ji, X. Wang, Y.P. Liao, W. Jiang, B. Sun, M.C. Hersam, A.E. Nel, T. Xia, Surface oxidation of graphene oxide determines membrane damage, lipid peroxidation, and cytotoxicity in macrophages in a pulmonary toxicity model, ACS Nano 12 (2) (2018) 1390–1402.
[23] S.P. Mukherjee, M. Bottini, B. Fadeel, Graphene and the immune system: a romance of many dimensions, Front. Immunol. 8 (2017) 11.
[24] D. Xue, E. Chen, H. Zhong, W. Zhang, S. Wang, M.U. Joomun, T. Yao, Y. Tan, S. Lin, Q. Zheng, Z. Pan, Immunomodulatory properties of graphene oxide for osteogenesis and angiogenesis, Int. J. Nanomed. 13 (2018) 5799–5810.
[25] J. Ma, R. Liu, X. Wang, Q. Liu, Y.N. Chen, R.P. Valle, Y.Y. Zuo, T. Xia, S.J. Liu, Crucial role of lateral size for graphene oxide in activating macrophages and stimulating pro-inflammatory responses in cells and animals, ACS Nano 9 (10) (2015) 10498–10515.
[26] C. Hoyle, J. Rivers-Auty, E. Lemarchand, S. Vranic, E. Wang, M. Buggio, N.J. Rothwell, S.M. Allan, K. Kostarelos, D. Brough, Small, thin graphene oxide is anti-inflammatory activating nuclear factor erythroid 2-related factor 2 via metabolic reprogramming, ACS Nano 12 (12) (2018) 11949–11962.
[27] J. Yi, G. Choe, J. Park, J.Y. Lee, Graphene oxide-incorporated hydrogels for biomedical applications, Polym. J. 52 (8) (2020) 823–837.
[28] R. Abdollahi, M.T. Taghizadeh, S. Savani, Thermal and mechanical properties of graphene oxide nanocomposite hydrogel based on poly (acrylic acid) grafted onto amylose, Polym. Degrad. Stabil. 147 (2018) 151–158.
[29] F. Olate-Moya, L. Arens, M. Wilhelm, M.A. Mateos-Timoneda, E. Engel, H. Palza, Chondroinductive alginate-based hydrogels having graphene oxide for 3D printed scaffold fabrication, ACS Appl. Mater. Interfaces 12 (4) (2020) 4343–4357.
[30] S. Liu, C. Zhou, S. Mou, J. Li, M. Zhou, Y. Zeng, C. Luo, J. Sun, Z. Wang, W. Xu, Biocompatible graphene oxide–collagen composite aerogel for enhanced stiffness and in situ bone regeneration, Mater. Sci. Eng. C 105 (2019), 110137.
[31] M. Wang, Y. Niu, J. Zhou, H. Wen, Z. Zhang, D. Luo, D. Gao, J. Yang, D. Liang, Y. Li, The dispersion and aggregation of graphene oxide in aqueous media, Nanoscale 8 (30) (2016) 14587–14592.
[32] M. Wang, B. Gao, D. Tang, H. Sun, X. Yin, C. Yu, Effects of temperature on aggregation kinetics of graphene oxide in aqueous solutions, Colloids Surf. A Physicochem. Eng. Asp. 538 (2018) 63–72.
[33] H. Bai, C. Li, X. Wang, G. Shi, On the gelation of graphene oxide, J. Phys. Chem. C 115 (13) (2011) 5545–5551.
[34] A.F. Girão, G. Gonçalves, K.S. Bhangra, J.B. Phillips, J. Knowles, G. Irurueta, M.K. Singh, I. Bdkin, A. Completo, P.A. Marques, Electrostatic self-assembled graphene oxide-collagen scaffolds towards a three-dimensional microenvironment for biomimetic applications, RSC Adv. 6 (54) (2016) 49039–49051.
[35] S.D. Purohit, R. Bhaskar, H. Singh, I. Yadav, M.K. Gupta, N.C. Mishra, Development of a nanocomposite scaffold of gelatin–alginate–graphene oxide for bone tissue engineering, Int. J. Biol. Macromol. 133 (2019) 592–602.
[36] R. Ma, Y. Wang, H. Qi, C. Shi, G. Wei, L. Xiao, Z. Huang, S. Liu, H. Yu, C. Teng, Nanocomposite sponges of sodium alginate/graphene oxide/polyvinyl alcohol as potential wound dressing: in vitro and in vivo evaluation, Compos. B Eng. 167 (2019) 396–405.
[37] M. Cacaci, C. Martini, C. Guarino, R. Torelli, F. Bugli, M. Sanguinetti, Graphene Oxide Coatings as Tools to Prevent Microbial Biofilm Formation on Medical Device, Advances in Microbiology, Infectious Diseases and Public Health, 2019, pp. 21–35.
[38] B. Hinz, D. Lagares, Evasion of apoptosis by myofibroblasts: a hallmark of fibrotic diseases, Nat. Rev. Rheumatol. 16 (1) (2020) 11–31.
[39] C. Gerarduzzi, J.A. Di Battista, Myofibroblast repair mechanisms post-inflammatory response: a fibrotic perspective, Inflamm. Res. 66 (6) (2017) 451–465.
[40] I.A. Darby, B. Laverdet, F. Bonté, A. Desmoulière, Fibroblasts and myofibroblasts in wound healing, Clin. Cosmet. Invest. Dermatol. 7 (2014) 301.

[41] X. Tong, J. Jiang, D. Zhu, F. Yang, Hydrogels with dual gradients of mechanical and biochemical cues for deciphering cell-niche interactions, ACS Biomater. Sci. Eng. 2 (5) (2016) 845–852.
[42] S. Asano, S. Ito, K. Takahashi, K. Furuya, M. Kondo, M. Sokabe, Y. Hasegawa, Matrix stiffness regulates migration of human lung fibroblasts, Physiol. Rep. 5 (9) (2017), e13281.
[43] A. Dey, X. Varelas, K.-L. Guan, Targeting the Hippo pathway in cancer, fibrosis, wound healing and regenerative medicine, Nat. Rev. Drug Discov. 19 (7) (2020) 480–494.
[44] S. Li, C. Li, Y. Zhang, X. He, X. Chen, X. Zeng, F. Liu, Y. Chen, J. Chen, Targeting mechanics-induced fibroblast activation through CD44-RhoA-YAP pathway ameliorates crystalline silica-induced silicosis, Theranostics 9 (17) (2019) 4993.
[45] S. Noguchi, A. Saito, T. Nagase, YAP/TAZ signaling as a molecular link between fibrosis and cancer, Int. J. Mol. Sci. 19 (11) (2018) 3674.
[46] S. Kim, C. Choi, C. Cha, Mechanotopography-driven design of dispersible nanofiber-laden hydrogel as a 3D cell culture platform for investigating tissue fibrosis, Adv. Health. Mater. 10 (21) (2021), 2101109.
[47] Y. Xu, G. Shi, J. Tang, R. Cheng, X. Shen, Y. Gu, L. Wu, K. Xi, Y. Zhao, W. Cui, ECM-inspired micro/nanofibers for modulating cell function and tissue generation, Sci. Adv. 6 (48) (2020), eabc2036.
[48] T.A. Wynn, L. Barron, Macrophages: Master Regulators of Inflammation and Fibrosis, Seminars in Liver Disease, © Thieme Medical Publishers, 2010, pp. 245–257.
[49] K.Y. Lee, M1 and M2 polarization of macrophages: a mini-review, Med. Biol. Sci. Eng. 2 (1) (2019) 1–5.
[50] J. Kzhyshkowska, A. Gudima, V. Riabov, C. Dollinger, P. Lavalle, N.E. Vrana, Macrophage responses to implants: prospects for personalized medicine, J. Leukoc. Biol. 98 (6) (2015) 953–962.
[51] Y.S. Lee, S.J. Song, H.K. Hong, B.Y. Oh, W.Y. Lee, Y.B. Cho, The FBW7-MCL-1 axis is key in M1 and M2 macrophage-related colon cancer cell progression: validating the immunotherapeutic value of targeting PI3Kgamma, Exp. Mol. Med. 52 (5) (2020) 815–831.
[52] L. Gao, W. Zhang, W.Q. Zhong, Z.J. Liu, H.M. Li, Z.L. Yu, Y.F. Zhao, Tumor associated macrophages induce epithelial to mesenchymal transition via the EGFR/ERK1/2 pathway in head and neck squamous cell carcinoma, Oncol. Rep. 40 (5) (2018) 2558–2572.
[53] V. Malheiro, F. Lehner, V. Dinca, P. Hoffmann, K. Maniura-Weber, Convex and concave micro-structured silicone controls the shape, but not the polarization state of human macrophages, Biomater. Sci. 4 (11) (2016) 1562–1573.
[54] T. Liu, L. Zhang, D. Joo, S.-C. Sun, NF-κB signaling in inflammation, Signal Transduct. Targeted Ther. 2 (1) (2017) 1–9.
[55] J. Ma, R. Liu, X. Wang, Q. Liu, Y. Chen, R.P. Valle, Y.Y. Zuo, T. Xia, S. Liu, Crucial role of lateral size for graphene oxide in activating macrophages and stimulating pro-inflammatory responses in cells and animals, ACS Nano 9 (10) (2015) 10498–10515.
[56] R. Li, L.M. Guiney, C.H. Chang, N.D. Mansukhani, Z. Ji, X. Wang, Y.-P. Liao, W. Jiang, B. Sun, M.C. Hersam, Surface oxidation of graphene oxide determines membrane damage, lipid peroxidation, and cytotoxicity in macrophages in a pulmonary toxicity model, ACS Nano 12 (2) (2018) 1390–1402.
[57] S.P. Mukherjee, B. Lazzaretto, K. Hultenby, L. Newman, A.F. Rodrigues, N. Lozano, K. Kostarelos, P. Malmberg, B. Fadeel, Graphene oxide elicits membrane lipid changes and neutrophil extracellular trap formation, Chem 4 (2) (2018) 334–358.
[58] Y. Tan, A. Suarez, M. Garza, A.A. Khan, J. Elisseeff, D. Coon, Human fibroblast-macrophage tissue spheroids demonstrate ratio-dependent fibrotic activity for in vitro fibrogenesis model development, Biomater. Sci. 8 (7) (2020) 1951–1960.
[59] S. Ricard-Blum, G. Baffet, N. Théret, Molecular and tissue alterations of collagens in fibrosis, Matrix Biol. 68 (2018) 122–149.
[60] J. Li, C. Zhou, C. Luo, B. Qian, S. Liu, Y. Zeng, J. Hou, B. Deng, Y. Sun, J. Yang, N-acetyl cysteine-loaded graphene oxide-collagen hybrid membrane for scarless wound healing, Theranostics 9 (20) (2019) 5839.
[61] J. Schoon, B. Hesse, A. Rakow, M.J. Ort, A. Lagrange, D. Jacobi, A. Winter, K. Huesker, S. Reinke, M. Cotte, Metal-specific biomaterial accumulation in human peri-implant bone and bone marrow, Adv. Sci. 7 (20) (2020), 2000412.
[62] R. Liu, S. Chen, P. Huang, G. Liu, P. Luo, Z. Li, Y. Xiao, Z. Chen, Z. Chen, Immunomodulation-based strategy for improving soft tissue and metal implant integration and its implications in the development of metal soft tissue materials, Adv. Funct. Mater. 30 (21) (2020), 1910672.
[63] N. Noskovicova, B. Hinz, P. Pakshir, Implant fibrosis and the underappreciated role of myofibroblasts in the foreign body reaction, Cells 10 (7) (2021) 1794.
[64] M. Al-Jarsha, V. Moulisová, A. Leal-Egaña, A. Connell, K.B. Naudi, A.F. Ayoub, M.J. Dalby, M. Salmerón-Sánchez, Engineered coatings for titanium implants to present ultralow doses of BMP-7, ACS Biomater. Sci. Eng. 4 (5) (2018) 1812–1819.
[65] V. Meretoja, S. Rossi, T. Peltola, L. Pelliniemi, T. Närhi, Adhesion and proliferation of human fibroblasts on sol-gel coated titania, J. Biomed. Mater. Res. 95 (1) (2010) 269–275.
[66] A.K. Refai, M. Textor, D.M. Brunette, J.D. Waterfield, Effect of titanium surface topography on macrophage activation and secretion of proinflammatory cytokines and chemokines, J. Biomed. Mater. Res. Part A: An Official Journal of The Society for Biomaterials, The Japanese Society for Biomaterials, and The Australian Society for Biomaterials and the Korean Society for Biomaterials 70 (2) (2004) 194–205.
[67] P. Duarte, C. Serrão, T. Miranda, L. Zanatta, M. Bastos, M. Faveri, L. Figueiredo, M. Feres, Could cytokine levels in the peri-implant crevicular fluid be used to distinguish between healthy implants and implants with peri-implantitis? A systematic review, J. Periodontal. Res. 51 (6) (2016) 689–698.